

Effect of upstream meniscus shape on dynamic wetting and operating limits of Newtonian coating liquids in slot coating bead flows

Won-Gi Ahn, Si Hyung Lee, Jaewook Nam, See Jo Kim, Kwan-Young Lee, Hyun Wook Jung

© American Coatings Association 2018

Abstract The coating bead flow and operability window for Newtonian coating liquids are theoretically and experimentally investigated in the slot coating process, with a focus on the shape of the upstream meniscus and contact angles. From the flow visualization in the coating bead region, the contact angles of the upstream meniscus were measured by changing the flow rate and web speed under uniform operating conditions. It was confirmed that the dynamic contact angle is closely related to the capillary number in this process, based on the Hoffman–Voinov–Tanner model. The viscocapillary and two-dimensional Navier–Stokes models using the experimentally observed contact angles accurately predicted the coating bead dynamics and operability windows for two Newtonian liquids.

Keywords Slot coating, Upstream meniscus, Dynamic contact angle, Static contact angle, Operability window

Won-Gi Ahn and Si Hyung Lee have contributed equally to this study.

W.-G. Ahn, K.-Y. Lee, H. W. Jung (✉)
Department of Chemical and Biological Engineering, Korea University, Seoul 02841, Republic of Korea
e-mail: hwjung@grtrkr.korea.ac.kr

S. H. Lee
Samsung Advanced Institute of Technology (SAIT), Gyeonggi 16678, Republic of Korea

J. Nam
School of Chemical and Biological Engineering, Seoul National University, Seoul 08826, Republic of Korea

S. J. Kim
School of Mechanical Engineering, Andong National University, Andong 36729, Republic of Korea

Introduction

Dynamic wetting, which replaces the gas phase with the liquid phase at a solid substrate surface, is an interesting phenomenon in many industrial coating processes. For example, the surface properties of a coating layer can play a key role in determining wetting or dewetting behavior; therefore, wetting issues have been particularly explored in the liquid film coating fields.^{1–4} If liquid droplets are deposited on a solid surface, three distinct phases exist (solid, liquid, and gas). In this case, the wetting characteristic can be mainly scrutinized by the contact angle at the liquid–air interface.⁵ There are two kinds of contact angles of a coating liquid over a substrate: the static contact angle on a stationary wall and dynamic contact angle on a moving substrate. Fundamental hydrodynamics linked with the wetting phenomenon and contact angle has been elucidated, both experimentally^{6,7} and theoretically.^{6,8} However, it is not easy to observe each contact angle for a liquid placed on a solid surface in the real coating processes.

The wetting states are related by capillary number (Ca), $Ca \equiv \mu U / \sigma$, where μ is the liquid viscosity, U is the moving substrate or web speed, and σ is the surface tension of the liquid. When Ca is very low ($Ca \rightarrow 0$), the dynamic contact angle approaches the static contact (equilibrium) angle on the substrate.⁹ According to the Hoffman–Voinov–Tanner model, the dynamic contact angle (θ) is correlated with Ca and equilibrium contact angle (θ_e).¹⁰

$$\theta^3 - \theta_e^3 \cong c_t Ca \quad (1)$$

where c_t is a constant (~ 72). As the moving web speed increases, the dynamic contact angle gradually increases up to 180° for large Ca . The contact angle of a liquid is mainly concentrated on the spreading of the liquid droplet on a solid surface. Although the role of

the contact angle in the coating processability and product quality control is very important in industrial coating processes, such as slot, curtain, slide, and roll coatings, this has been the least concern in practical operations. In particular, the wettability of a coating liquid in the slot coating process, which is widely used in producing lithium-ion batteries, solar cells, catalytic filters, and displays, should be carefully considered.

In the slot coating process, both static and dynamic contact angles in a dynamic wetting region exist, called the coating bead region, which is enclosed by die lips, free surface menisci at the upstream and downstream sides, and moving web (Fig. 1).^{11–13} In Fig. 1, a static contact line with static contact angle (ϕ) is located on the upstream die lip wall and a dynamic contact line having dynamic contact angle (θ) meets a surface of moving web in the upstream region. Here, the length from the inner corner of the upstream die lip to the static contact line is defined as l_s , and the length from the dynamic contact line to the static contact line is defined as Δx . The upstream meniscus generated by the two contact lines and free surface is a crucial factor in deciding the stable operating conditions.^{14,15} The flow dynamics in the coating bead is also affected by the dynamic and static contact angles.^{10,16–18} Didari et al.¹⁹ and Bhamidipati et al.²⁰ eloquently investigated wetting behavior for complex coating liquids in slot coatings. Vandre et al.²¹ studied the effect of meniscus confinement on the wetting failure using a hydrodynamic model and compared wetting failure phenomena, such as saw-tooth.

In this study, the effect of contact angles of the upstream free surface in the coating bead region on the upstream meniscus shape and operability window is investigated by finding the dependence of Ca in the Newtonian slot coating process. In order to reliably

observe the contact angles of upstream meniscus, a flow visualization technique was performed by changing the web speed and flow rate injected into the slot die; then, these results were compared with the lubrication approximation and two-dimensional (2-D) simulations. A transient condition, where the shape of the upstream meniscus changed from concave to convex, can be found by changing the process conditions including Ca . It was substantiated that the operability window could be more accurately predicted from the viscocapillary and 2-D models when the contact angle data from the experiments were correctly applied.

Experimental setup

Properties of coating liquids

Two different Newtonian coating liquids were prepared to investigate the wetting dynamics in the coating bead region. The Newtonian liquids were mixtures of glycerin and water (i.e., GW82 = 80:20 and GW91 = 90:10 in weight percent ratios). The physical and rheological properties of the coating liquids are listed in Table 1. Their shear viscosity and surface tension were measured using a rotational rheometer (AR2000, TA Instruments) and a surface tension meter (DCAT11, Dataphysics), respectively.

Slot coating flow experiments

Flow visualization in the coating bead region was carried out by continuously coating liquids on a steel

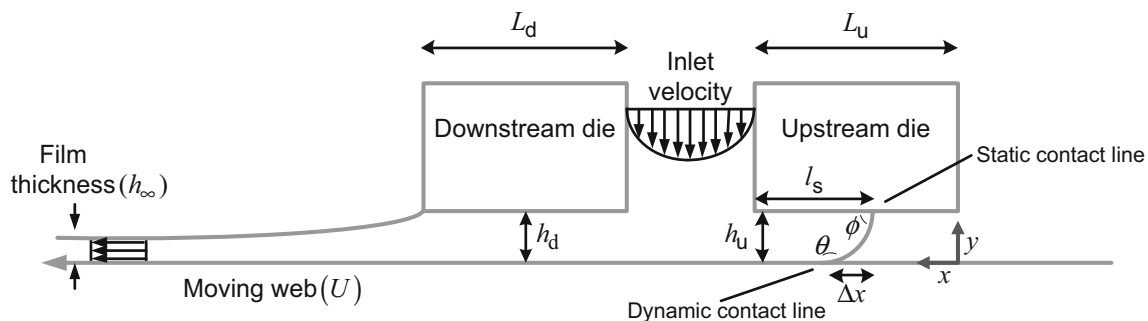


Fig. 1: Schematic diagram of slot coating bead region

Table 1: Physical and rheological properties of coating liquids used in this study

Coating liquid (glycerin/water, wt%)	Density (kg/m ³)	Surface tension (N/m)	Viscosity (Pa·s)
GW82	1210	0.066	0.045
GW91	1232	0.0645	0.145

roll, as schematically similar in Ji et al.²² The coating liquid was controlled by a gear pump (Cole-Parmer, gear pump system, SN-74014-25). It is distributed and metered within the die manifold and deposited on the roll surface. Then, it was removed from the roll surface by a blade and stored in a storage tank.

The position and shape of the upstream meniscus in the coating bead region were observed for establishing the operability windows and determining the contact angles at upstream meniscus. To reliably capture the upstream meniscus for static and dynamic contact angles, a CCD camera with the resolution of 1920 x 1080 pixels and frame rate of 63 Hz (Prosilica GX 1910C, Allied Vision) and a custom-made XYZ-stage device (Sciencetown, Korea) were installed close to the side of the slot die coater. First, operability windows for the two liquids were experimentally constructed by observing the position of the upstream meniscus using the CCD camera, which is dependent on the flow rate and web speed; that is, the onsets for leaking and bead breakup were determined when the position of the upstream meniscus was located far upstream and near feed in the upstream die lip, respectively.^{12,13} (For example, leaking and bead breakup onsets can be found by gradually decreasing and increasing web speed, respectively, based on the stable condition at the constant flow rate.) Next, contact angles, which are closely related to Ca, were measured through two experimental pathways within uniform operating regions. One method was to simultaneously change the flow rate and web speed while maintaining the upstream meniscus position. The other method was to gradually increase the web speed at constant flow rates. The dimensions of the slot die were as follows: width (W_d) of 50 mm, slit gap (W_s) of 500 μm , upstream (L_u) and downstream (L_d) die lip lengths of 1000 μm , and upstream (h_u) and downstream (h_d) coating gaps of 200 μm . Various spatial dimensions for upstream meniscus such as l_s and Δx are decided from the image analysis of captured images in the coating bead region.

Numerical simulations for coating bead flows

A simplified viscocapillary model to characterize the coating bead flow was adopted in this study and was basically derived from 2-D equations by means of the lubrication approximation.^{12,13} The viscocapillary models in slot coating systems reasonably and reliably predict flow behavior and operability windows, agreeing with the experimental data.^{11,12,22–24}

As the coating bead flow is primarily affected by the pressure gradient and drag driven by the moving web, the flow field and pressure distribution in the coating bead can be approximated at the upstream and downstream regions. The final viscocapillary model (Eq. 2) applied here, which is a relationship between

the position of the upstream meniscus and ambient pressures outside the coating bead, is completed by additionally applying the Young–Laplace equation and the Landau–Levich approximation for the upstream and downstream menisci, respectively, under no bead pressure condition.

$$x_f - x_u = \frac{h^2}{6\mu U} \left(-1.34\text{Ca}^{2/3} \frac{\sigma}{h_\infty} + \frac{\sigma}{h} (\cos \theta + \cos \phi) \right) - L_d \left(1 - \frac{2h_\infty}{h} \right) \quad (2)$$

where x_u indicates the upstream meniscus position in an x -coordinate with the origin at the outer corner of upstream die lip in a positive direction, x_f is the feed position (slit exit), $h = h_d = h_u$, and h_∞ is the final wet thickness. More detailed procedures to derive the approximate model for Newtonian coating liquids were introduced in Lee et al.¹³

Operability windows obtained from the viscocapillary model and experiments were compared with those predicted by two-dimensional (2-D) calculation based on the Galerkin finite element method (FEM) developed in Lee et al.^{13,25} The Navier–Stokes equation for the 2-D coating bead flow is as follows.

$$\rho \frac{D\mathbf{v}}{Dt} = -\nabla P + \mu \nabla^2 \mathbf{v} + \rho \mathbf{g} \quad (3)$$

where \mathbf{v} indicates the velocity vector, P the isotropic pressure, ρ the liquid density, \mathbf{g} the gravitational acceleration. To calculate free surfaces, the following elliptic partial differential equations should be satisfied.

$$\nabla \cdot (D_\xi \nabla \xi) = 0 \text{ and } \nabla \cdot (D_\eta \nabla \eta) = 0 \quad (4)$$

where D_ξ and D_η are diffusion-like coefficients incorporated to control spacing grids. The weak forms of equations (3)–(4) must satisfy the inverse mapping from the physical domain (x, y) to the computational domain (ξ, η). The coating bead flow including velocity, pressure, and meniscus position in the physical domain is evaluated by the above method with the following boundary conditions: static and dynamic contact angles assigned at upstream meniscus, slip condition for the dynamic contact line, no-slip on die lips and moving web, total stress jump conditions due to the surface tension, and kinematic boundary of no-flow across free surfaces.^{12,13,26,27} Note that a downstream contact line was pinned to the downstream die lip for simply calculating 2-D coating bead region. The number of elements in the simulation domain was 1964, guaranteeing the numerical accuracy. The shapes of the upstream meniscus from the flow visualization and 2-D FEM were also compared in various cases.

Results and discussion

Operability windows by models and experiments

The operability windows for the two coating liquids were established from the viscocapillary and 2-D models on the basis of the position of the upstream meniscus by gradually changing the flow rate and web speed in the low Ca regime (Fig. 2a). The static and dynamic contact angles for Fig. 2 were set to 60° and 120°, respectively, as per the usual conditions^{12,13,22,25}; however, these were replaced later by the experimentally observed ones. The onsets of leaking were decided when the upstream static contact line was positioned on the upper edge of the upstream die lip. Note that finding leaking onsets experimentally was not easy because of the difficulty in pinning the upstream meniscus at the outer corner of the upstream die lip. In addition, the onsets of the bead breakup were determined when the upstream static contact line was located on the edge of the feed slot.

We reformulated experimental onsets in Fig. 2b in terms of dimensionless critical wet thickness and Ca to address the contact angle effect in low Ca region,

exhibiting the very similar results between onsets of bead breakup and minimum wet thickness from Lee et al.²⁸ under no bead pressure condition. A limit of two liquids might be merged in single lines, regardless of liquid viscosity. It is also found that a thin coating layer less than half of the coating gap can be produced in the region of low Ca and bead breakup defect occurs when the wet thickness is half of the coating gap as the ratio increases, as remarked in the basic lubrication approximation.

The role of the upstream meniscus in determining the operability windows was reasonably verified in many cases.^{14,25} For example, Figs. 2c and 2d show the positions and shapes of the upstream meniscus at the stable and near bead breakup cases, respectively, at the constant flow rate.

The predicted operability windows from both the viscocapillary and 2-D models were identical. However, there was a slight difference in the operability limits between the models and experiments; the GW91 liquid had a slightly wider uniform region in comparison with the GW82 liquid from the simulations, whereas the experimentally determined uniform regions for the GW82 liquid were wider than those of the

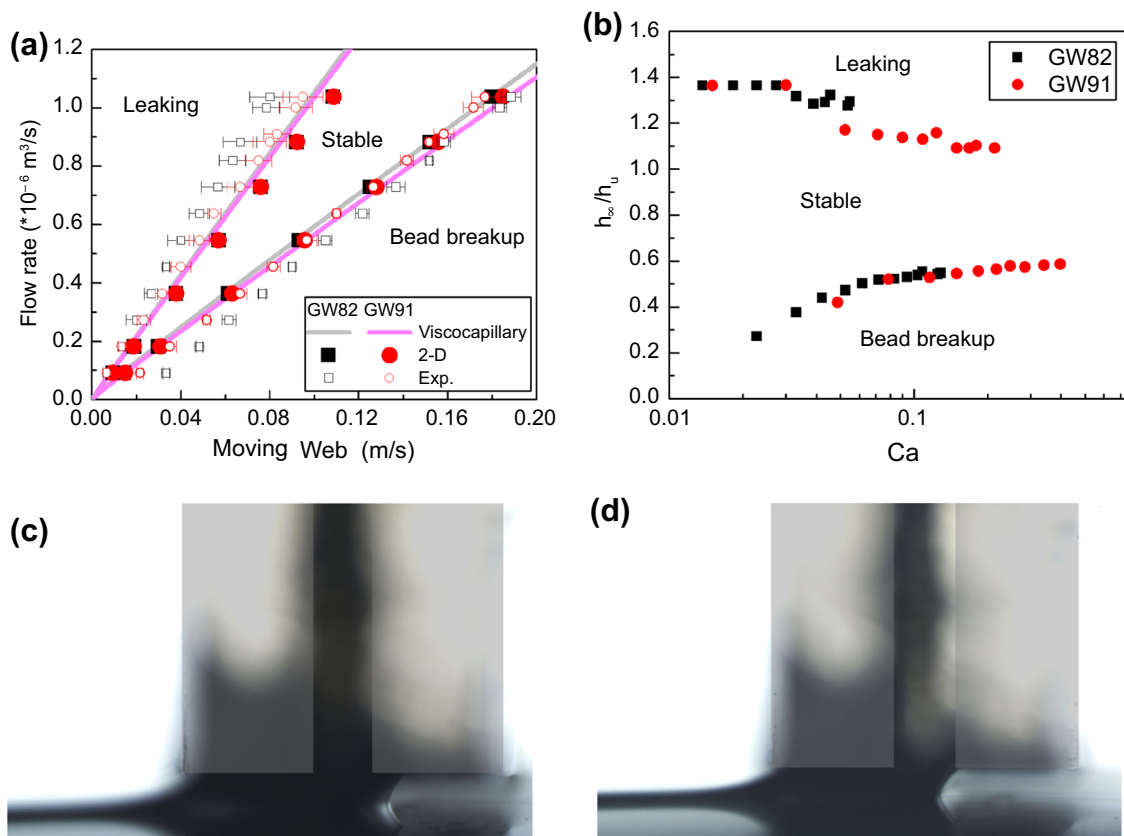


Fig. 2: (a) Operability windows for two coating liquids obtained from simulations and experiments. Static and dynamic contact angles used in simulations were 60° and 120°, respectively. (b) Experimental critical wet thickness data near the onsets along Ca. Flow images captured at (c) stable (Flow rate = $0.18 \times 10^{-6} \text{ m}^3/\text{s}$, web speed = 0.045 m/s) and (d) bead breakup states (Flow rate = $0.18 \times 10^{-6} \text{ m}^3/\text{s}$, web speed = 0.048 m/s)

GW91 liquid. This discrepancy might be due to the different contact angles for the two liquids from the experiments, especially in the very low Ca region. Under very low web speed conditions, the contact angles will be noticeably changed, according to the variation of flow rate and web speed, producing a difference in the operability windows of the simulations and experiments. Therefore, the actual contact angles acquired from the visualization for the various conditions should be correctly incorporated into the simulations to accurately portray the coating bead dynamics and windows for rheologically different coating liquids.

Observation of upstream meniscus shape

The shape of the upstream meniscus in the coating bead region was observed from the visualization method. The experimental points for GW91 and GW82 designated in Fig. 3a were in stable conditions. As mentioned in the slot coating flow experiments section, for the first method, the flow rate and web speed were simultaneously varied (see symbols), while

maintaining the position of the upstream meniscus (the length, l_s , was almost 106.0 μm for GW82 and 287.9 μm for GW91). Note that the position of the upstream meniscus was not exactly the same because its positions were very sensitive with respect to a small change in web speed at low Ca. The resulting wet thickness at symbols is not constant (Fig. 3b) because the relation between flow rate and web speed is not linear in Fig. 3a. To quantitatively check the upstream meniscus position and shape for the two liquids, the lengths, l_s and Δx , and contact angles, θ and ϕ , were directly obtained from the meniscus images captured from a CCD camera. In the second method, the web speed was changed under the constant flow rates in the uniform operating range (see solid and dashed lines). The upstream meniscus moved along the upstream die lip, free from coating defects within the onsets of leaking and bead breakup.

Figure 3c shows the change in the dynamic contact angle along Ca for the two coating liquids by the simultaneous variation of flow rate and web speed (the first method) in Fig. 3a. As Ca increased, the dynamic contact angle generally increased up to $\sim 160^\circ$. The dynamic contact angle conceptually satisfies the Hoff-

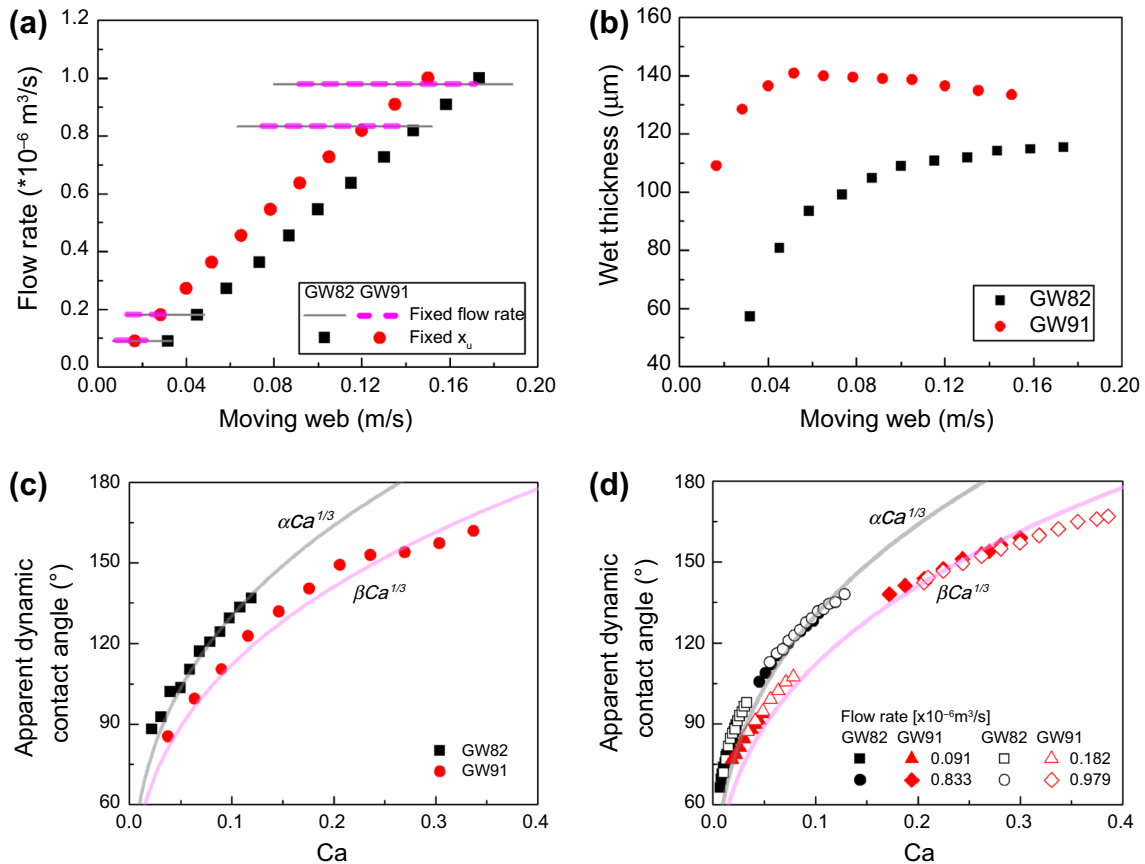


Fig. 3: (a) Experimental routes for directly observing contact angles in the coating bead. (b) Wet thickness condition by method 1 (simultaneous change in both flow rate and web speed under fixed meniscus position). Dynamic contact angle data by experimental (c) method 1 and (d) method 2 (web speed change at constant flow rates)

man–Voinov–Tanner relation (i.e., $\theta^3 \propto Ca$) in the slot coating flows. Figure 3d also shows the change in dynamic contact angle along Ca for the two liquids by varying the web speed at constant flow rates (the second method), as shown in Fig. 3a. Although the range of contact angle for a uniform coating at a given flow rate was different for each case, these data interestingly fall on corresponding single curves along Ca . The trend of increasing contact angle in this case is quantitatively similar to that in Fig. 3c, indicating that the dynamic contact angle is strongly correlated with Ca .

The wetting dynamics are closely related to the ranges of Ca . Changes in both contact angle and meniscus shape along Ca are also schematically delineated in Fig. 4a. In our experiments, the shapes of the upstream menisci for the GW82 and GW91 liquids changed from concave to linear, and further to convex, as Ca increased (Figs. 4b and 4c). A Ca condition exists that is associated with a linear meniscus shape from the wetting mechanism. In these cases, the shape of the

upstream meniscus tended to have a linear form for the two coating liquids when Ca was close to 0.1.

Comparison of coating bead flows from experiments and 2-D simulations

The dynamic (θ) and static (ϕ) contact angles of upstream meniscus observed from the captured images were incorporated into 2-D computations for a comparison with the experimental results. The length scales, l_s and Δx , for the upstream meniscus were compared from both the simulations and experiments under the same operating conditions. The experimental data, including the shapes and positions of the upstream meniscus, quantitatively agreed with the 2-D simulations, as shown in Figs. 5 and 6 for GW82 and GW91, respectively.

When Ca was very low at the same upstream meniscus position for the GW82 case (Fig. 5a), a feed vortex or recirculation was generated, even in the

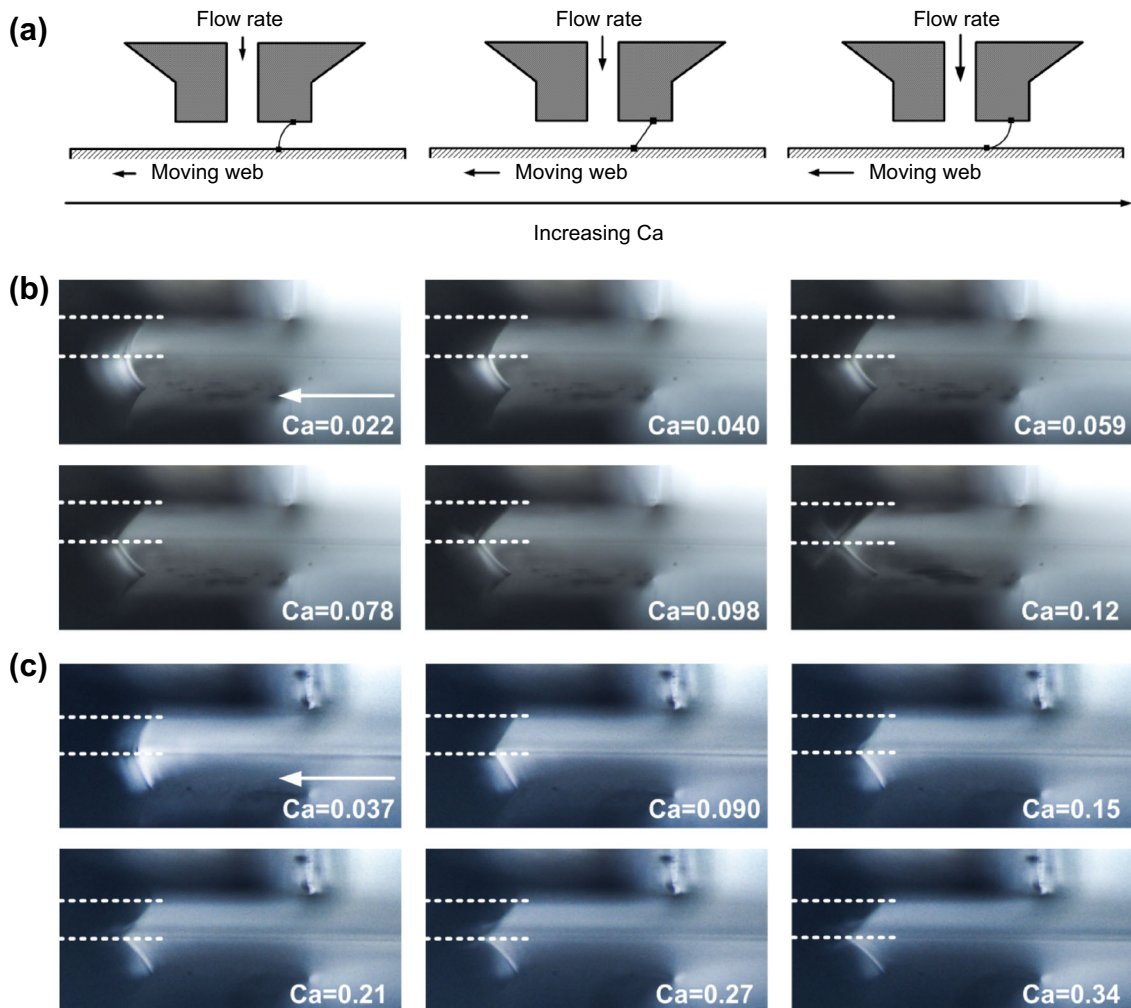


Fig. 4: (a) Schematic change (from concave to convex) of upstream meniscus shape with increasing Ca . Experimental observations of upstream meniscus for (b) GW82 and (c) GW91 liquids at different Ca values

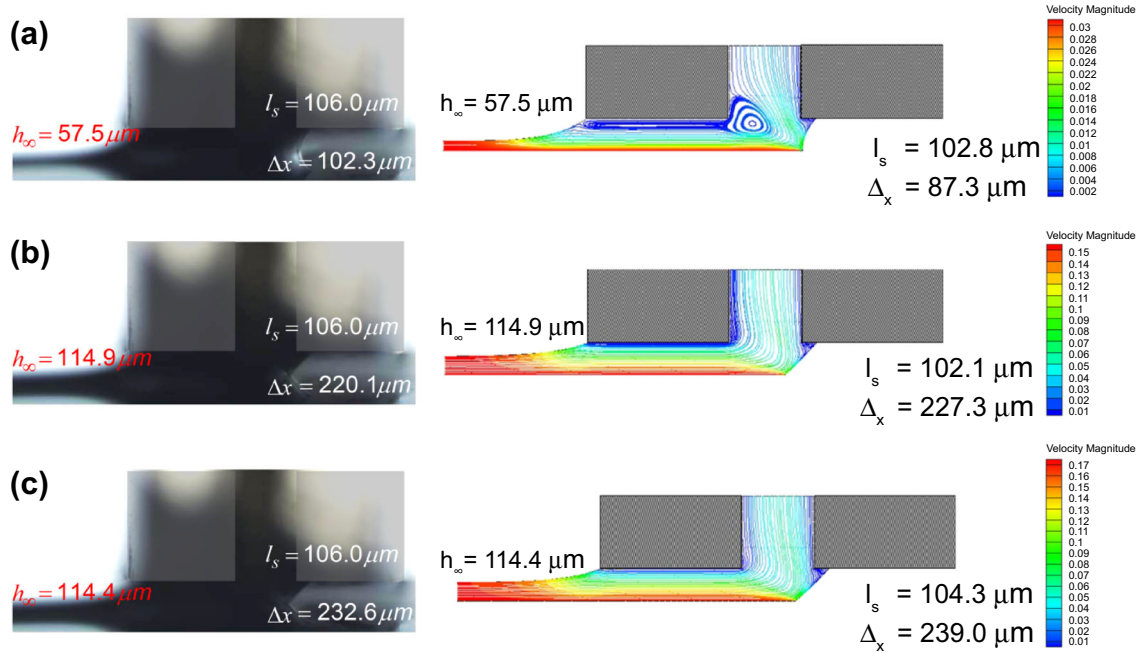


Fig. 5: Comparison of flow patterns from experiments and 2-D simulations experimental observation at different Ca values for GW82 liquid. (a) Ca = 0.0216, (b) Ca = 0.108, and (c) Ca = 0.118

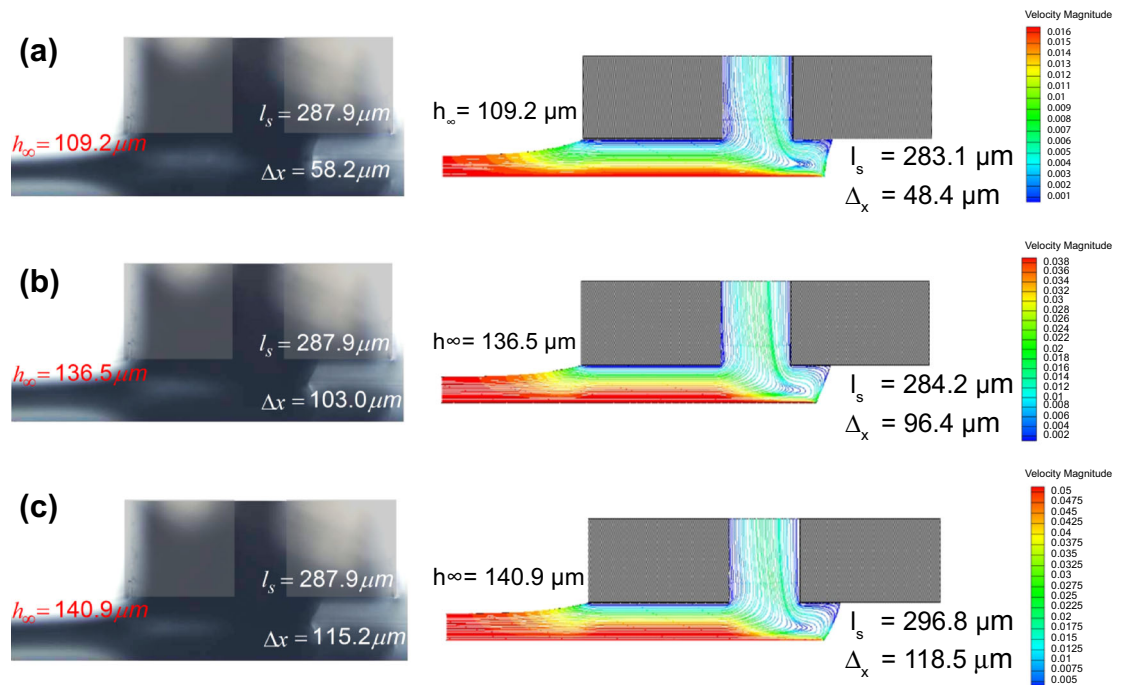


Fig. 6: Comparison of flow patterns from experiments and 2-D simulations experimental observation at different Ca values for GW91 liquid. (a) Ca = 0.0375, (b) Ca = 0.0899, and (c) Ca = 0.116

stable operating state. It is well known that a feed vortex is predicted when the final wet thickness is less than 1/5 of the slit gap (500 μm), and the downstream die lip vortex occurs when the final wet thickness is less

than one-third of the downstream coating gap.²⁹ When the final coating thickness is less than half of the downstream coating gap under the no bead pressure condition, the coating system is likely to be unsta-

ble.^{12,13} Although the final thickness ($h_\infty = 57.5 \mu\text{m}$) was less than half of the coating gap ($h_0 = 200 \mu\text{m}$), the coating system was still stable, as experimentally and theoretically depicted in Fig. 5a, which is related to the formation of upstream meniscus with relatively low static and dynamic contact angles. Therefore, a thin film coating will be possible by controlling the wetting characteristics without the help of a vacuum box.

Effect of contact angles at upstream meniscus on coating bead dynamics

The dynamic or static contact angles were arbitrarily varied to determine the changes in the coating bead flow (Fig. 7) under the same flow rate and web speed conditions. As the dynamic or static contact angle decreased, the position of the upstream meniscus moved outward of the upstream die lip to match the equilibrium pressure between the liquid and air, even though the operating conditions were the same, except for the contact angles. From these results, it is found that a thinner final coating thickness is possible by further increasing the moving web by tuning the contact angle properties, because the stability of the coating bead flow is closely related to the position of the upstream meniscus.^{12–14} In this case, the feed and downstream vortices are naturally formed in the production of the very thin coating layer.

Effect of contact angles at upstream meniscus on operability window

To illustrate the effect of the contact angles on the uniform coating operation, experimentally observed angles were introduced to the viscocapillary and 2-D models for reconstructing the operability coating window which was first shown in Fig. 2a. As discussed above, the upstream meniscus position was influenced by the contact angles. Therefore, the contact angle data must be precisely acquired from the visualization of the coating bead flow for a better estimation of the operability coating windows.

Figure 8 shows the static and dynamic contact angles measured near the onsets of bead breakup under several flow rate conditions (0.091×10^{-6} , 0.182×10^{-6} , 0.819×10^{-6} , and $1.001 \times 10^{-6} \text{ m}^3/\text{s}$), among data of Fig. 3d. Note that the leaking onset was not considered in this section because of the difficulty in capturing the contact angles at the leaking onset. Employing the curve-fitting functions of these contact angles at the bead breakup onsets, the operability windows for the two coating liquids are reproduced in Fig. 9. The bead breakup onsets were well predicted from both the viscocapillary and 2-D models, taking the experimental contact angles into account. Note that the viscocapillary model could be usefully applied to Ca range up to 0.4 in this study, which is known to be limited within $Ca = 0.1$. From these

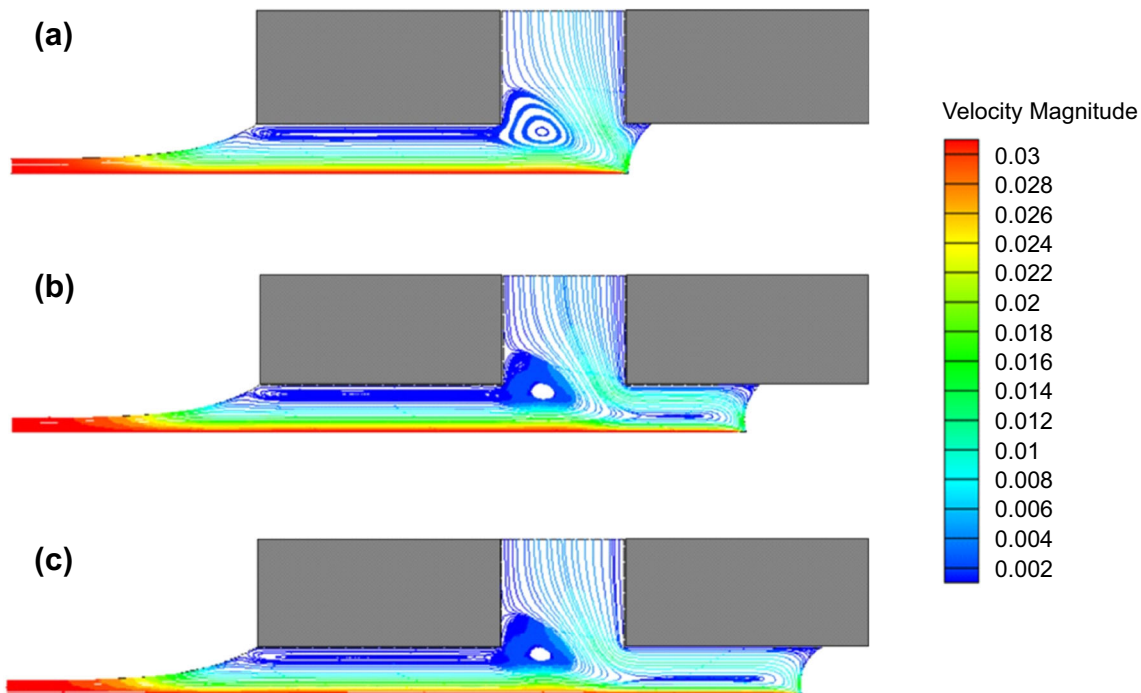


Fig. 7: Effect of contact angles on coating bead flow of GW82 liquid with $h_\infty = 57.5 \mu\text{m}$ under same flow rate ($0.091 \times 10^{-6} \text{ m}^3/\text{s}$) and web speed (0.032 m/s) conditions. (a) $\theta = 88.2^\circ$, $\phi = 43.8^\circ$, (b) $\theta = 70^\circ$, $\phi = 43.8^\circ$, and (c) $\theta = 70^\circ$, $\phi = 30^\circ$

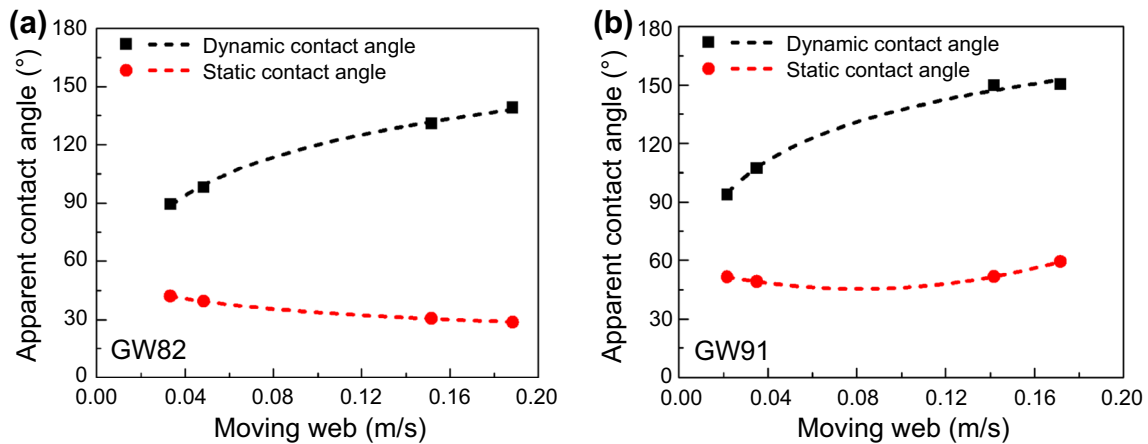


Fig. 8: Dynamic and static contact angles at bead breakup onsets for (a) GW82 and (b) GW91 liquids

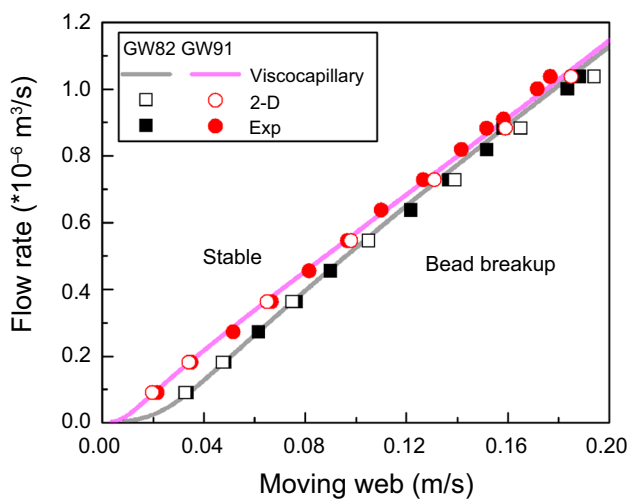


Fig. 9: Comparison of bead breakup limits from experiment and simulations. Contact angle data observed from experiments were employed in the simulations

results, it was confirmed that the operability coating window can be better established by implementing the actual contact angle data, especially in not high Ca region where the contact angle is rather sensitive to the operating conditions. It would be worthwhile mentioning that this approach will be favorably applied to non-Newtonian coating liquid systems.

Conclusion

The shape and contact angles of the upstream meniscus were observed from a CCD camera in the coating bead region for elucidating the effect of the contact angles (mainly the dynamic contact angle) on the flow dynamics and operability window in the slot coating systems. The position of the upstream meniscus, regarded as an indicator for determining the operability window, is affected by the contact angles formed in

the upstream meniscus, especially in the low Ca region. The meniscus shape changed from concave to linear, and further to convex as Ca increased, resulting in an increased contact angle. It was confirmed that the dynamics contact angle of the upstream meniscus measured under various conditions within the uniform flow states was closely related to Ca, qualitatively satisfying the Hoffman–Voinov–Tanner relation. A uniform thin coating layer could be produced without the bead pressure application by controlling the wetting characteristics. The operability windows for two Newtonian liquids were theoretically established by adopting experimentally observed contact angles, and employing the simplified viscocapillary and 2-D Navier–Stokes models. The operability windows from both models and experiments showed reasonably good agreement.

Acknowledgments This work was supported by the National Research Foundation of Korean (NRF) grant funded by the Korean government (MSIP) (NRF-2016R1A5A1009592) and the Ministry of Trade, Industry & Energy (MOTIE, Korea) under the Industrial Technology Innovation Program (No.10067706).

References

1. Durian, DJ, Franck, C, “Wetting Phenomena of Binary Liquid Mixtures on Chemically Altered Substrates.” *Phys. Rev. Lett.*, **59** (5) 555–558 (1987)
2. Extrand, CW, Kumagai, Y, “An Experimental Study of Contact Angle Hysteresis.” *J. Colloid Interface Sci.*, **191** (2) 378–383 (1997)
3. Kistler, SF, Schweizer, PM, *Liquid Film Coating*. Chapman & Hall, London (1997)
4. Blake, TD, Shikhmurzaev, YD, “Dynamic Wetting by Liquids of Different Viscosity.” *J. Colloid Interface Sci.*, **253** (1) 196–202 (2002)

5. Ruijter, D, Michel, J, Blake, TD, Coninck, JD, “Dynamic Wetting Studied by Molecular Modeling Simulations of Droplet Spreading.” *Langmuir*, **15** (22) 7836–7847 (1999)
6. Tanner, LH, “The Spreading of Silicone Oil Drops on Horizontal Surfaces.” *J Phys. D. Appl. Phys.*, **12** (9) 1473–1484 (1979)
7. Huppert, HE, “The Propagation of Two-Dimensional and Axisymmetric Viscous Gravity Currents Over a Rigid Horizontal Surface.” *J. Fluid Mech.*, **121** 43–58 (1982)
8. Voinov, OV, “Hydrodynamics of Wetting.” *Fluid Dyn.*, **11** (5) 714–721 (1976)
9. Bonn, D, Eggers, J, Indekeu, J, Meunier, J, Rolley, E, “Wetting and Spreading.” *Rev. Mod. Phys.*, **81** (2) 739–805 (2009)
10. Hoffman, RL, “A Study of the Advancing Interface. I. Interface Shape in Liquid–Gas Systems.” *J. Colloid Interface Sci.*, **50** (2) 228–241 (1975)
11. Higgins, BG, Scriven, LE, “Capillary-Pressure and Viscous Pressure-Drop Set Bounds on Coating Bead Operability.” *Chem. Eng. Sci.*, **35** (3) 673–682 (1980)
12. Gates, ID, “Slot Coating Flows: Feasibility, Quality.” PhD Thesis, University of Minnesota, 1999
13. Lee, SH, Koh, HJ, Ryu, BK, Kim, SJ, Jung, HW, Hyun, JC, “Operability Coating Windows and Frequency Response in Slot Coating Flows Using Viscocapillary Model.” *Chem. Eng. Sci.*, **66** (21) 4953–4959 (2011)
14. Nam, J, Carvalho, MS, “Two-Layer Tensioned-Web-Over-Slot Die Coating: Effect of Operating Conditions on Coating Window.” *Chem. Eng. Sci.*, **65** (13) 4065–4079 (2010)
15. Lee, YW, Ahn, WG, Nam, J, Jung, HW, “Operability Windows in Viscoelastic Slot Coating Flows Using a Simplified Viscoelastic-Capillary Model.” *Rheol. Acta*, **56** (9) 707–717 (2017)
16. Huh, C, Scriven, LE, “Hydrodynamic Model of Steady Movement of a Solid/Liquid/Fluid Contact Line.” *J. Colloid Interface Sci.*, **35** (1) 85–101 (1971)
17. Kistler, SF, “Hydrodynamics of Wetting.” *Wettability*, **6** 311–430 (1993)
18. Ding, X, Liu, J, Harris, TAL, “A Review of the Operating Limits in Slot Die Coating Processes.” *AIChE J.*, **62** (7) 2508–2524 (2016)
19. Didari, S, Ahmad, ZY, Veldhorst, JD, Harris, TAL, “Wetting Behavior of the Shear Thinning Power Law Fluids.” *J. Coat. Technol. Res.*, **11** (1) 95–102 (2014)
20. Bhamidipati, KL, Didari, S, Bedell, P, Harris, TAL, “Wetting Phenomena During Processing of High-Viscosity Shear-Thinning Fluid.” *J. Non-Newtonian Fluid Mech.*, **166** (12) 723–733 (2011)
21. Vandre, E, Carvalho, MS, Kumar, S, “Delaying the Onset of Dynamic Wetting Failure Through Meniscus Confinement.” *J. Fluid Mech.*, **707** 496–520 (2012)
22. Ji, HS, Ahn, WG, Kwon, I, Nam, J, Jung, HW, “Operability Coating Window of Dual-Layer Slot Coating Process Using Viscocapillary Model.” *Chem. Eng. Sci.*, **143** 122–129 (2016)
23. Ruschak, KJ, “Limiting Flow in a Pre-metered Coating Device.” *Chem. Eng. Sci.*, **31** (11) 1057–1060 (1976)
24. Koh, HJ, Kwon, I, Jung, HW, Hyun, JC, “Operability Window of Slot Coating Using Viscocapillary Model for Carreau-Type Coating Liquids.” *Korea-Aust. Rheol.*, **24** (2) 137–141 (2012)
25. Lee, SH, Kim, SJ, Nam, J, Hyun, WJ, Hyun, JC, “Effect of Sloped Die Lip Geometry on the Operability Window in Slot Coating Flows Using Viscocapillary and Two-Dimensional Models.” *J. Coat. Technol. Res.*, **11** (1) 47–55 (2014)
26. De Santos, JM, “Two-Phase Concurrent Downflow Through Constricted Passage.” PhD Thesis, University of Minnesota, 1991
27. Carvalho, MS, “Roll Coating Flows in Rigid and Deformable Gap.” PhD Thesis, University of Minnesota, 1996
28. Lee, KY, Liu, LD, Liu, TJ, “Minimum Wet Thickness in Extrusion Slot Coating.” *Chem. Eng. Sci.*, **47** (7) 1703–1713 (1992)
29. Sartor, L, “Slot Coating: Fluid Mechanics and Die Design.” PhD Thesis, University of Minnesota, 1990